Neuronal Lipoprotein Lipase Deficiency alters Neuronal Function and Hepatic Metabolism

Kimberley Bruce (kimberley.bruce@ucdenver.edu)
University of Colorado https://orcid.org/0000-0001-5656-1534
Hong Wang
University of Colorado Denver - Anschutz Medical Campus
Evgenia Dobrinskikh
University of Colorado Denver - Anschutz Medical Campus
Ivan A Rudenko
University of Colorado Denver - Anschutz Medical Campus
Hong Gao
Tulane University
Andrew E Libby
Georgetown University Medical Center
Sachi Gorkhali
University of Colorado Denver - Anschutz Medical Campus
Tian Yu
University of Colorado Denver - Anschutz Medical Campus
Andrea Zsombok
Tulane University
Robert H Eckel
University of Colorado Denver - Anschutz Medical Campus

Research

Keywords: Lipoprotein Lipase, neuronal metabolism, fatty liver, Brain-liver-axis.

Posted Date: February 26th, 2020

DOI: https://doi.org/10.21203/rs.2.24553/v1

Version of Record: A version of this preprint was published at Metabolites on September 28th, 2020. See the published version at https://doi.org/10.3390/metabo10100385.

Abstract

Background: The autonomic regulation of hepatic metabolism offers a novel target for the treatment of non-alcoholic fatty liver disease (NAFLD). However, the molecular characteristics of neurons that regulate the brain-liver axis remain unclear. Since mice lacking neuronal lipoprotein lipase (LPL) develop perturbations in neuronal lipid-sensing and systemic energy balance, we reasoned that LPL may be a component of pre-autonomic neurons involved in the regulation of hepatic metabolism. Methods: Measures of glucose homeostasis in mice homozygous (NEXLPL-/-) and heterozygous (NEXLPL+/-) for neuronal LPL deficiency were compared to that of WT mice. A detailed analysis of hepatic glucose and lipid metabolism was also determined in NEXLPL+/- at 6-18 mo. To determine the effect of neuronal LPL deficiency on neuronal physiology, liver-related neurons were identified in the paraventricular nucleus (PVN) of the hypothalamus using the transsynaptic retrograde tracer PRV-152. In addition, we used Fluorescence Lifetime Imaging Microscopy (FLIM) as a novel method to visualize changes in neuronal metabolism following LPL-depletion directly in the PVN. Results: Here we show that despite obesity, mice with reduced neuronal LPL also show improved glucose tolerance and reduced hepatic lipid accumulation with aging, concomitant with reduced hepatic lipogenic gene expression (e.g. SCD1 and FADS2). Retroviral tracing and patch clamp studies revealed reduced inhibitory post-synaptic currents in liver-related neurons lacking LPL. Quantification of the free versus bound Nicotinamide Adenine Dinucleotide (NADH) and Flavin Adenine Dinucleotide (FAD), revealed that LPL loss resulted in altered substrate utilization characterized by increased glucose utilization and TCA cycle flux. These findings were recapitulated by analysis of global metabolites from hypothalamic cell lines either deficient in, or over-expressing, LPL. Conclusions: Our data suggest that LPL is a novel feature of liver–related preautonomic neurons in the PVN. Moreover, LPL loss is sufficient to alter neuronal metabolism and function, leading to changes in systemic glucose metabolism including improved hepatic function with age.

1. Background

The liver is central to the pathogenesis of metabolic disorders such as obesity, type 2 diabetes mellitus (T2DM), and cardiovascular disease. It is thought that hepatic lipid accumulation precedes insulin resistance (1, 2), which plays a pivotal role in the development of T2DM (3). Importantly, hepatic neutral lipid accumulation and the incidence of non-alcoholic fatty liver disease (NAFLD) increase markedly with age (4). Thus, preventing hepatic fat accumulation is a promising strategy to prevent age-associated metabolic disease. The autonomic nervous system (ANS) plays a key role in regulating hepatic metabolism (5), and is therefore an attractive target for the treatment of metabolic disease. Metabolic signals from the hypothalamus reach the liver via neuronal pathways that include the brain stem, sympathetic nerves, and vagus nerve. However, the metabolic characteristics of hypothalamic preautonomic neurons remain undefined.

The accumulation of intermediary metabolites in specific brain regions can alter hepatic metabolism, suggesting that the brain-liver axis is involved in responding to nutrient status and maintaining whole-

body energy homeostasis. For example, central administration of glucose stimulates the conversion of lactate to pyruvate and activates a K_{ATP} channel–dependent pathway within the hypothalamus, leading to lowered VLDL-TG secretion from the liver and reduced circulating triglycerides (TG) (6). In addition, fatty acids (FA) such as oleic acid activate a PKC-δ - K_{ATP} channel signaling pathway, resulting in suppressed VLDL-TG secretion in rats (7). This signaling requires the dorsal vagal complex, highlighting a brain-liver neurocircuitry in which hypothalamic FA-sensing triggers a hepatic-neuronal relay to regulate hepatic lipid homeostasis (7). However, the precise cellular components involved in neuronal FA sensing remain unclear. While several FA transporters have been identified in the brain, these are only associated with specific FA species and do not account for the unique composition of lipid substrates in the brain, i.e. glial-derived lipoproteins. For example, CD36 knock-out mice show reduced monounsaturated FA incorporation into brain phospholipids, but no changes in essential polyunsaturated fatty acids (PUFA) concentration (8), suggesting that alternative pathways may regulate PUFA uptake and metabolism.

We and others have previously shown that lipoprotein lipase (LPL)—the rate-limiting enzyme in the hydrolysis of TG-rich lipoproteins and FA uptake—is involved in neuronal lipid uptake and the co-ordination of systemic metabolism (9–13). Specifically, mice homozygous and heterozygous for pan-neuronal LPL deficiency (NEXLPL-/- and NEXLPL+/-) develop obesity with aging (6 mo. and 12 mo. respectively), and a specific PUFA deficiency associated with neurobehavioral abnormalities (11, 13). Thus, based on the systemic impact of neuronal LPL deficiency we reasoned that neuronal LPL may play a role in hypothalamic lipid-sensing and the ANS regulation of hepatic metabolism. In the present study, we demonstrate that obese mice with neuronal LPL deficiency show preserved glucose tolerance with age, involving reduced hepatic lipid accumulation and altered activity of liver-related neurons in the PVN. Moreover, LPL loss is sufficient to alter neuronal metabolism and function, which may precede changes in systemic metabolism including preserved hepatic function with age.

2. Materials And Methods

Animals

All animal procedures where performed in accordance with institutional regulations at the University of Colorado School of Medicine. Male NEXLPL-/-, NEXLPL+/- and WT mice were generated as previously described and housed in standard conditions, fed standard laboratory chow diet until terminal experiments at 3 mo. (WT n= 4, NEXLPL-/- n=4), 6 mo. (WT n= 8, NEXLPL-/- n=6, NEXLPL+/- n =6), 12 mo (WT n= 3, NEXLPL-/- n=5, NEXLPL+/- n =5), 18 mo. (WT n= 6, NEXLPL-/- n=5, NEXLPL+/- n =6) (11). Mice were fasted for four hours prior to tissue harvest. Body composition was measured on anesthetized mice by dual-energy x-ray absorptiometry using a mouse densitometer (PIXImus2, Lunar Corp., Madison, WI). The electrophysiological studies were conducted at Tulane University. The procedures were approved by the Institutional Animal Care and Use Committee.

Glucose and insulin tolerance tests

Glucose and insulin tolerance tests were performed by bolus intraperitoneal injection of glucose (1 g/kg) or insulin (0.75 units/kg), respectively. Blood glucose was measured from the tail using a glucometer (OneTouch Ultra, Lifescan) at baseline (0) and 10, 20, 30, 45, 60, and 90 min after injection.

Hyperinsulinemic-euglycemic clamps

Before the clamp experiment, mice were fasted overnight. On the day of the clamp experiment, mice were anesthetized and an indwelling catheter was inserted in the right internal jugular vein (14). A three-way connector was attached to the catheter to intravenously deliver solutions. A 2-hour hyperinsulinemic-euglycemic clamp was conducted in all four groups of mice with a primed (150 mU/kg body wt) and continuous infusion of insulin (Humulin; Eli Lilly, Indianapolis, IN) at a rate of 2.5, 5 or 10 mU/kg/min to raise plasma insulin within a physiological range. 20% glucose was infused at variable rates to maintain glucose at basal concentrations. Blood samples (10 µl) were collected at 10 min intervals for measurement of plasma glucose concentration only. Basal and insulin stimulated whole-body glucose turnover were estimated with a continuous infusion of [3-^{3}H]glucose (PerkinElmer, Boston, MA) for 2 h before the clamps (0.05 µCi/min) and throughout the clamps (0.1 µCi/min), respectively. To estimate insulin-stimulated glucose uptake in individual organs, 2-deoxy-D-[1- ^{14}C] glucose (2-[^{14}C]-DG) was administered as a bolus (10 µCi) when euglycemic clamp has approached. 10 min after 2-[^{14}C]-DG being injected, tissues were taken for biochemical analysis.

Analysis of liver lipids

Neutral lipid was analyzed as described previously (15-17). Frozen liver tissue was homogenized in (v/v) Folch reagent (2:1 CHCl3/MeOH) containing 300 mg of tritridecanoin reference standard (Nu-Check Prep Inc., Elysian, MN) by bead homogenization for two cycles of 2 min at 30 Hz. Homogenates were diluted further with Folch reagent to 4 ml, treated with 800 ml of 0.9% sodium chloride solution, vortexed, and centrifuged at 4000 rpm for 5 min. The organic phase was removed and dried under N2 gas. Total lipids were resuspended in 330 ml of 100% chloroform and applied to HyperSep SI SPE columns (Thermo Scientific, Waltham, MA) pre-equilibrated with 15 column volumes chloroform. Neutral lipids were eluted with a total of 3 ml of chloroform, dried under N2, and resuspended in 1 ml of methanol containing 2.5% H2 SO4 . Fatty acid methyl ester (FAME) production was initiated by heating at 80 °C for 1.5 h. 1 ml of HPLC-grade water was added to quench the reactions, and FAMEs/cholesterol was extracted with 200 ml of hexane. A Trace 1310 GC with a TG-5MS column (Thermo Scientific, Waltham, MA) was used to separate lipids chromatographically, and lipids were analyzed with an ISQ single quadrupole mass

spectrometer. Xcalibur software (Thermo Scientific) was used to calculate peak areas. Areas were normalized to the tritridecanoin reference standard and then to tissue weight. Histological analysis and scoring of hepatic lipids and steatosis were performed as previously described (18).

Lipoprotein Profile

Plasma samples (200 µL) were chromatographed via fast protein liquid chromatography (FPLC) using two Superose 6 columns in series as previously reported (19). Cholesterol was measured in each fraction using a commercially available kit (Cayman Chemical Company, Ann Arbor, MI, USA) following procedures outlined in the package insert.

Quantitative real-time PCR

Total RNA was reverse transcribed with the iScript cDNA synthesis kit (Bio-Rad, Hercules, CA). Quantitative PCR was performed using primer sets for genes of interest and reference genes (designed using NCBI's Primer3/BLAST) and iTaq Universal SYBR Green Supermix (Bio-Rad) following manufacturer's protocols. Reactions were run in duplicate on an iQ5 Real Time PCR detection system (Bio-Rad) along with a no-template control per gene. Validation experiments were performed to demonstrate that efficiencies of target and reference genes were approximately equal. Data were normalized to two reference genes (*GAPDH* and *ACTB*) using the comparative Ct method.

Identification of liver-related neurons with PRV-152

Retrogradely transported pseudorabies viral vector (PRV-152, provided by the Center for Neuroanatomy with Neurotropic Viruses) expressing enhanced green fluorescent protein (EGFP) was used to identify liver-related neurons (20-22). Under anesthesia, the liver was exposed with a small transverse incision and ~4 ml of PRV-152 was injected into the median lobe of the liver (2 injections of 2 sites). A drop of adhesive "liquid bandage" was used to seal each injection to prevent the leakage of the virus. The animals were maintained in a biosafety level 2 facility up to 110 h post-injection.

Brain slice preparation

Acute brain slices were prepared from WT and NEXLPL-/- mice. After anesthesia with isoflurane, the brain was removed and immersed in ice-cold oxygenated artificial cerebrospinal fluid (aCSF) containing the following (in mM): 124 NaCl, 26 $NaHCO_3$, 1.4 NaH_2PO_4, 11 glucose, 3 KCl, 1.3 $MgCl_2$, 1.5 $CaCl_2$, pH 7.3-7.4. Transverse hypothalamic slices containing the PVN (300mm) were made using a vibrating microtome. The slices were stored in a holding chamber at 34-36°C, and then transferred to a recording chamber mounted on a fixed stage under an upright microscope (Nikon FN1).

Whole-cell patch-clamp recordings

Whole-cell patch-clamp recordings were performed at 34-36°C from liver-related neurons in the PVN identified under 40x water-immersion objective (N.A=0.8). Epifluorescence was used to identify EGFP-containing neurons and infrared illumination and differential interference contrast optics (IR-DIC) to target specific cells. For whole-cell patch-clamp recordings, electrodes (3-7 MW) were filled with a solution containing the following (in mM): 130 Cs^+ gluconate, 10 HEPES, 5 EGTA, 1 NaCl, 1 $MgCl_2$, 1 $CaCl_2$, 3 CsOH , 2-3 Mg-ATP, 0.2% biocytin, pH 7.3-7.4. Electrophysiological signals were recorded using an Axoclamp 700B amplifier (Molecular Devices) and acquired by pClamp (Molecular Devices). Inhibitory post-synaptic currents (IPSCs) were recorded at -10 mV and excitatory post-synaptic currents (EPSCs) at -60 mV. Data were analyzed offline using pClamp or MiniAnalysis (Synaptosoft).

Stereotaxic AVV injection

Adeno-associated virus 8 coding for Cre recombinase and GFP under control of CaMKIIa promoter (AAV8-CaMKIIa-GFP-Cre, UNC viral core) was utilized to achieve recombination between flox sites of PVN neurons. Adeno-associated virus 8 coding for GFP under control of CaMKIIa promoter (AAV8-CaMKII-GFP, UNC viral core) was used as control vector (mice referred to as PVN nLPL+). 10-week old male LPL flox/flox mice were anesthetized with 2.0% isoflurane and surgical anesthesia plane was maintained with 1.0% isoflurane. Incision site was locally anesthetized with 100-200 µl of lidocaine (1 mg/mL). Mice were then mounted onto stereotaxic apparatus (Neurostar). 100 nL of virus was injected bilaterally into the PVN (anteroposterior −0.7 mm, lateral +/- 0.25 mm, and dorsoventral −4.8 mm) using 0.5 µl Hamilton syringe (part# 86250, Hamilton Company) at a rate of 20 nL/min (23). Syringe was kept in place for 5 minutes after each infusion and the needle was withdrawn over 3 minutes. 2 weeks following the initial injection, anesthetized mice were transcardially perfused with HBSS (with calcium and Magnesium) and whole brains were fresh-frozen in liquid nitrogen-cooled 2-methylabutane, since fixed brains are incompatible with Fluorescence Lifetime Imaging Microscopy.

Fluorescence Lifetime Imaging Microscopy (FLIM)

FLIM was performed to detect local metabolic changes in 5-7 different areas of PVN in a fresh brain sections using a Zeiss 780 laser-scanning confocal/multiphoton-excitation fluorescence microscope with a 34-Channel GaAsP QUASAR Detection Unit and non-descanned detectors for 2-photon fluorescence (Zeiss, Thornwood, NY) equipped with an ISS A320 FastFLIM box and a titanium:sapphire Chameleon Ultra II (Coherent, Santa Clara, CA). The 2-photon excitation was blocked by a 2-photon emission filter. For the acquisition of FLIM images, fluorescence for Nicotinamide Adenine Dinucleotide (NADH) and Flavin Adenine Dinucleotide (FAD) was detected simultaneously by two photon-counting PMT detectors (H7422p-40; Hamamatsu). Images of the different areas of PVN in the brains were obtained with Vista Vision software by ISS in 256x256 format with a pixel dwell time of 6.3 µs/pixel and averaging over 30 frames. Calibration of the system was performed by measuring the known lifetime of the fluorophore fluorescein with a single exponential decay of 4.0 ns (24). The phasor transformation and data analysis were carried out using Global SimFCS software (Laboratory for Fluorescence Dynamics (LFD), University of California, Irvine) as described previously (25). The number of pixels covered with lifetimes for free and bound reduced form of NADH and FAD were calculated in SimFCS (LFD) and the values were normalized to the total number of pixels detected as previously described (26, 27).

The glycolytic index was calculated for all experimental groups using the following equation: as defined previously (27, 28).

Cell Culture conditions and Reagents

mHypoE41 (N41) immortalized mouse hypothalamic neurons were purchased from CELLutions Biosystems (Winnipeg, MB). N41 cells were grown in DMEM containing 1000 mg/L glucose and 10% FBS at 37°C in the presence of 5% CO_2. To produce cells for stable overexpression of LPL (N41 mLPL or Empty [control]), N41 cells were transduced with MSCV as previously described (10). To produce stable knock-down cells, N41 cells were transduced with shRNA (N41 553, or N41 202 [control]) containing lentivirus as previously described (10).

Metabolomics

Frozen cell pellets were extracted at 2e6 cells/mL in ice-cold lysis/extraction buffer (methanol:acetonitrile:water 5:3:2 v/v/v). Metabolites were separated using a 9-minute C18-based gradient method as described (29), using a Thermo Vanquish UHPLC coupled to a Thermo Q Exactive mass spectrometer. Amino acids (30), and other metabolites (31), were quantified as previously described.

Statistical analysis

For electrophysiological experiments, continuous recordings have been conducted and 2-minute periods were analyzed with MiniAnalysis (Synaptosoft) to measure peak amplitude and frequency of post-synaptic currents. Comparison between groups was made with an unpaired two-tailed Student's t test. For all analysis, $P<0.05$ was considered significance. Numbers are reported as mean ± standard error of mean (SEM).

Two-way repeated measure ANOVA was performed for all age and time related analysis, using post-hoc multiple comparison with Bonferroni correction, using GraphPad 7 data analysis and graphing software, with $P<0.05$ being considered significant and $P<0.1$ a trend.

3. Results

3.1 Neuronal LPL deficient mice have improved glucose tolerance

To investigate the effect of neuronal LPL deficiency on systemic and hepatic metabolism we raised a new cohort of NEXLPL-/-, NEXLPL+/- and WT mice. Prior to additional metabolic characterization we confirmed that the formerly observed phenotype had been recapitulated. Indeed, as previously described (15;17;19), NEXLPL-/- mice were heavier than WT controls by 12 mo. of age ($P < 0.001$ vs WT). By 12 mo. NEXLPL+/- mice were also heavier than WT controls, but to a lesser degree ($P < 0.01$ vs WT) (Fig. 1E).

To determine whether neuronal LPL deficiency could influence peripheral glucose homeostasis, we performed 2-hour intraperitoneal (IP) glucose tolerance tests (GTT). Both NEXLPL-/- and NEXLPL+/- mice showed improved glucose clearance by 6 mo., with lower plasma glucose concentrations at 2 hours ($P < 0.05$ versus WT) (Fig. 1B). Surprisingly, despite marked obesity at 12 mo., NEXLPL-/- mice showed improved glucose tolerance ($P < 0.01$ vs WT), a pattern also observed in the NEXLPL+/- mice ($P < 0.05$ vs WT) (Fig. 1C). Due to the degree of obesity and diminishing health of NEXLPL-/- mice at 18 mo. these mice were not studied, however, the NEXLPL+/- mice showed markedly improved glucose tolerance at 18 mo. compared to WT control mice, again despite increased body weight and fat mass ($P < 0.01$ vs WT) (Fig. 1D).

3.2 NEXLPL +/- mice have reduced hepatic glucose production

Since neuronal LPL deficiency is associated with improved glucose tolerance despite obesity, we reasoned that these animals may be more insulin sensitive. To test this, mice were given an IP bolus of insulin at 12 and 18 mo. of age; the time points at which the greatest differences in glucose tolerance were observed. Although both WT and NEXLPL+/- mice responded to the insulin bolus, this response was greater in the 12 mo NEXLPL+/- mice compared to WT ($P < 0.05$ at 20 and 30 minutes), and longer-lasting in the 18 mo NEXLPL+/- mice, with a trend for plasma glucose levels rising more rapidly in the WT controls ($P < 0.09$) (Fig. 1F).

In patients with T2DM, endogenous glucose production (EGP) is the primary factor responsible for elevations in fasting plasma glucose levels and contributes importantly to postprandial hyperglycemia. Thus, we hypothesized that the age-associated improvements in glucose tolerance observed in the NEXLPL-/- and NEXLPL+/- mice may be due to lower EGP. Hence, we performed hyperinsulinemic-euglycemic clamps to show that hepatic, but not systemic insulin sensitivity was increased in NEXLPL+/- mice compared to WT mice, an effect demonstrated at low physiological insulin infusion rates, i.e. 2.5 mg/kg/min (Fig. 1G). In addition, NEXLPL+/- mice showed an increased ability of insulin to suppress EGP at low insulin concentrations (Fig. 1H).

3.3 NEXLPL+/- mice have reduced hepatic lipid accumulation

Since hepatic lipid accumulation can precede changes in hepatic insulin sensitivity, we predicted the improved glucose tolerance and insulin sensitivity observed in mice lacking neuronal LPL may be a consequence of altered hepatic lipid metabolism. Thus, we performed histological analysis for hepatic steatosis in livers of 6 mo. old WT and NEXLPL+/- mice. Lipid droplets were clearly visible in WT liver sections, present as moderate macro and micro-vesicular steatosis (Fig. 2A), however relatively few lipid droplets were observed in the NEXLPL+/- mice (Fig. 2A).

We also observed a reduced total TG content in the livers of NEXLPL+/- mice at 6, 12 and 18 mo. (Fig. 2B). In fact, this decrease was observed in almost all lipid species (data not shown), with the greatest differences being observed in the monounsaturated (MUFA) content (Fig. 2C).

Since VLDL export from the liver is a major contributor towards hepatic lipid homeostasis we measured the plasma lipoprotein profile of NEXLPL+/- and WT mice at 18 mo. (Fig. 2D). We observed an increase in plasma VLDL-cholesterol concentrations in NEXLPL+/- vs WT mice ($P < 0.05$ vs WT) (Fig. 2E). Of note, low density lipoprotein (LDL) cholesterol concentrations were almost identical between the NEXLPL+/- and WT mice. However, plasma high-density lipoprotein (HDL) cholesterol was lower in the NEXLPL+/- mice ($P < 0.05$ vs WT) (Fig. 2E).

To further understand the mechanism behind altered lipid metabolism in the livers of mice lacking neuronal LPL, we measured the expression of genes key to hepatic lipid homeostasis. Stearoyl-CoA desaturase (SCD1), the rate limiting enzyme in MUFA synthesis showed an increasing trend of expression with age in all genotypes (Fig. 2F). However, SCD1 expression was lower in the livers of NEXLPL+/- mice compared to WT at 6, and 18 mo. ($P < 0.05$ vs WT) (Fig. 2F). In addition, fatty acid desaturase 2 (FADS2), which catalyzes the first and rate-limiting step in several fatty acid desaturation pathways showed a robust increase with age (Fig. 2G), halted in NEXLPL+/- mice at 12 mo. ($P < 0.05$ vs WT) (Fig. 2G).

3.4 Liver-related PVN neurons in NEXLPL-/- mice have reduced inhibitory synaptic control

A growing number of studies suggest that the activity of preautonomic neurons in the PVN of the hypothalamus have a pivotal role in the autonomic regulation of hepatic glucose and lipid metabolism (20, 32–34). Since synaptic inputs largely contribute to the excitability of neurons, we reasoned that the synaptic control of liver-related neurons in the PVN is altered in mice with neuronal LPL deficiency. Liver-related PVN neurons were identified with the retrograde transsynaptic viral tracer PRV-152 (Fig. 3A), and inhibitory and excitatory post-synaptic currents were recorded from EGFP expressing PVN neurons. The observed EGFP labeling indicated liver-related preautonomic neurons in the PVN (Fig. 3B), consistent with previous findings (20). Our data showed decreased spontaneous IPSC frequency in NEXLPL-/- mice compared with WT mice (Fig. 3C). The average frequency of sIPSCs was 0.97 ± 0.07 Hz in NEXLPL-/- mice; while 3.56 ± 0.93 Hz in WT mice suggesting that inhibitory neurotransmission to liver-related PVN neurons is reduced in NEXLPL-/- mice ($P < 0.05$) (Fig. 3D). In contrast, we did not find significant differences in excitatory neurotransmission ($P > 0.05$).

3.5. Loss of LPL in PVN neurons alters metabolic flux

We have previously shown that neuronal LPL plays an important role in neuronal lipid sensing, however, the mechanism underlying this process remains unknown. Since the canonical role of LPL is to facilitate cellular lipid uptake, we hypothesized that LPL loss may alter neuronal metabolism, which may be linked to observed changes in synaptic control. A major limiting factor regarding metabolic studies in neurons is the ability to preserve endogenous metabolism at the time of quantification, without causing major changes during ex-vivo culture. Indeed, many primary cultures of neurons are from the early post-natal period, and endogenous metabolism may differ vastly from that in the adult mouse. Here, we employed Fluorescence Lifetime Imaging Microscopy (FLIM) as a novel method to measure the endogenous metabolic status of neurons from fresh frozen brain tissue with high spatial resolution. LPL was depleted in neurons of the PVN in $LPL^{flox/flox}$ mice using adenoviral delivery of a GFP-Cre virus, driven by the neuronal specific CamKIIα promoter (Fig. 4A). GFP allowed for localization to the PVN (Fig. 4A), and to neurons (Fig. 4B), which is essential since fixation and/or staining abolishes the ability to measure and discriminate between the lifetimes of NADH and FAD co-enzymes. Overall, we showed that there was a significant shift towards free versus bound NADH in LPL deficient PVN neurons ($P < 0.05$) (Fig. 4D), which indicates increased flux through metabolic pathways producing free NADH (e.g. glycolysis), rather than

flux through metabolic pathways in which NADH would be bound to metabolic enzymes (i.e. oxidative phosphorylation). Moreover, there was a dramatic shift in the proportion of free FAD versus bound FAD ($P < 0.001$) (Fig. 4E), which suggests an increase in processes that produce free FAD (e.g. TCA), and a reduction in process in which enzymes utilize FAD as cofactor (e.g. oxidative phosphorylation and FA oxidation).

To validate changes in substrate utilization following LPL loss, we measured global metabolites in hypothalamic neuronal cell lines in which LPL was either depleted (LPL KO N41) or over-expressed (LPL OE N41). Although immortalized or primary cell lines cannot perfectly recapitulate the in vivo studies described above, this established cell tool enables us to validate major changes in metabolic pathways following LPL loss. Here, we found a marked increase in the abundance of fructose 1-6-bisphosphate in LPL KO N41 neurons compared to control neurons ($P < 0.001$) (Fig. 5A and Supplemental Fig. 1 https://figshare.com/s/d125253ec0dfc4eafc81). Although this suggests an increase in glucose utilization following LPL loss via glycolysis, it also indicates increased flux through the pentose phosphate pathway (PPP); the preferred route of glucose utilization in neurons (35). Importantly both glycolysis and PPP are a source of free NADH, supporting the observation of increased free NADH following LPL loss (Fig. 4D). In addition, we found an increase in the abundance of TCA metabolites, such as malate ($P < 0.01$), fumarate ($P < 0.001$) and succinate ($P < 0.001$) (Fig. 5B and Supplemental Fig. 2 https://figshare.com/s/a17b4d86cb6dafe10949) in LPL KO N41 neurons, suggesting an augmented flux through this pathway and thus, increased free FAD production. Interestingly, LC-PUFAs were reduced in the LPL KO N41 neurons, but significantly increased in the LPL OE N41 neurons (Fig. 5C and Supplemental Fig. 3 https://figshare.com/s/cc5b4597659171c99eda). While this suggests that FA oxidation flux may be reduced, contributing to free FAD accumulation, it also highlights LPL's role in selective PUFA uptake and is consistent with previous studies (10, 11, 13).

4. Dicussion

Since aberrant hepatic glucose production and lipid metabolism play a key role in the development of metabolic diseases such as IGT, T2DM and even hypertriglyceridemia, identification of the mechanisms underlying the brain-liver axis holds promise for the development of novel interventions and therapeutics. Several studies have highlighted the ability of specific neuropeptides and metabolites to act upon key hypothalamic energy-sensing nuclei, and in turn modulate downstream metabolism (7, 36–38). However, how neurons receive such inputs is largely unknown. The goal of the present study was to investigate whether LPL was involved in the regulation of hepatic metabolism by modulating FA sensing in neurons. We reasoned that since the neuronal –specific LPL depletion (e.g. NEXLPL-/- and NEXLPL+/-) mice show hyperphagia, inactivity and obesity, autonomic regulation of the peripheral metabolic organs such as the liver was likely. Interestingly, we found that despite obesity mice with reduced neuronal LPL showed improved glucose tolerance with age; a phenotype that involves reduced hepatic EGP and preserved hepatic insulin sensitivity despite aging, and obesity.

Using GTTs in NEXLPL-/-, NEXLPL+/- and WT mice at several age points, we found that mice lacking neuronal LPL had improved glucose tolerance compared to WT controls, a key difference that became more pronounced with aging (Fig. 1). Importantly, by 12 mo., both the NEXLPL-/- and NEXLPL+/- mice were heavier than WT mice, however, glucose tolerance was preserved throughout age, despite obesity (Fig. 1). Although paradoxical, this phenotype is reminiscent of obese individuals who remain “metabolically healthy” (39). These insulin-sensitive obese (ISO) individuals have lower visceral fat accumulation, less ectopic fat, and less systemic inflammation than insulin-resistant obese individuals (40, 41). Interestingly, NEXLPL-/- and NEXLPL+/- mice exhibit brown adipose tissue hyperplasia (11), and NEXLPL+/- mice show reduced ectopic hepatic lipid accumulation (Fig. 2A), both hallmarks of ISO. In further support, here we show that NEXLPL+/- mice have improved hepatic insulin sensitivity (Fig. 2). Therefore, it is plausible that reductions in neuronal LPL influence the autonomic regulation of systemic metabolism to mimic the ISO individuals.

The autonomic regulation of hepatic glucose metabolism is well established. Several studies have demonstrated that stimulation of the splanchnic nerve modulates liver function (Sympathetic nervous system [SNS]) increases EGP and decreases glycogenesis, whereas stimulating the vagus nerve (parasympathetic nervous system [PNS]) decreases EGP and increases glycogenesis (42, 43). Since we observed lower EGP in mice with reduced neuronal LPL, it is tempting to speculate that we observe increased PNS activity in these animals compared to wild-type mice. However, we cannot rule out the possibility that changes in EGP are due to reduced SNS activity. Thus, further studies are needed to delineate this mechanism. Nonetheless, our findings strongly support the notion that LPL is a feature of preautonomic neurons involved in neuronal central lipid sensing and the regulation of hepatic glucose metabolism.

The ANS is also involved in the regulation of hepatic lipid metabolism. Here we show that the abundance of hepatic TG, MUFA (Fig. 2C), and the expression of SCD1 (Fig. 2F) and FADS2 (Fig. 2G), increases robustly with age in WT mice. This increase in hepatic lipid species is reminiscent of the increase in prevalence of NAFLD in the aging population (4). Since the SNS is dysregulated with age (44), and has been implicated in the development of NAFLD (45), our data point to an age-associated increase in SNS activity in WT mice. Importantly, mice that are heterozygous for neuronal LPL deficiency have reduced hepatic lipid accumulation, and lipogenic gene expression (Fig. 2) despite aging. Therefore, it is tempting to speculate that the loss of neuronal LPL dampens an age-associated rise in SNS activity with age. Since we observe a marked decrease in hepatic MUFA, and SCD1, the enzyme responsible for the formation of mono-unsaturated acyl-CoAs from saturated acyl-CoAs, this highlights a lipogenic pathway regulated by neuronal LPL loss. This is consistent with previous studies in which liver lipids were altered following differential metabolic sensing in the brain. Specifically, central administration of glucose has been shown to mimic the ‘fed state’ in the brain and lower hepatic SCD1 activity leading to reduced MUFA synthesis (6).

Preautonomic neurons in the PVN are known to contribute to the ANS regulation of hepatic metabolism (46). Here, we identified liver-related PVN neurons and determined their synaptic regulation in mice

lacking neuronal LPL. Our data clearly showed reduced sIPSCs in liver-related PVN neurons in NEXLPL-/- mice ($P < 0.05$ vs WT) (Fig. 3C), strongly suggesting that the inhibitory synaptic regulation of liver-related PVN neurons is altered in NEXLPL-/- mice. Although further studies are needed to elucidate the mode of neurotransmission, studies have highlighted the role of GABAergic inhibition in the regulation of preautonomic neurons. For example, blockade of $GABA_A$ receptors in the PVN caused a pronounced increase in plasma glucose concentration via sympathetic nerves to the liver (34). This suggests that reduced inhibition of sympathetic PVN neurons may be detrimental to glucose homeostasis. However, at this stage we cannot delicate whether neuronal LPL deficiency results in decreased inhibition of pre-sympathetic or pre-parasympathetic neurons.

It is also plausible to suggest that the altered neuronal metabolism could result in changes to synaptic function. To monitor changes in neuronal metabolism ex vivo, we employed FLIM to measure both NADH and FAD lifetime changes following LPL loss. Although an established method for measuring endogenous metabolism (47, 48), this methodology has not previously been used to further our understanding of neuronal metabolism. Here, we clearly show that free NADH is increased in LPL deficient PVN neurons (Fig. 4D). Typically, this would suggest an increased flux through glycolysis (49–51). However, since neurons have a limited capacity to up-regulate glycolysis (52), increased glucose utilization through the PPP in neurons is more likely (35). In further support of this interpretation, we also observed a marked increase in fructose-1-6 bisphosphate in LPL-deficient hypothalamic neurons (Fig. 5A). Due to the lack of 6-phosphofructo-2-kinase/fructose-2, 6-bisphosphatase-3 ((Pfkfb3), fructose-6P, cannot be shuttled through traditional glycolytic routes, and instead is converted to fructose-1-6 bisphosphate and shunted towards the PPP (53). Therefore, an accumulation of fructose-1-6 bisphosphate suggests an increase in glucose uptake, whether this also suggests a block in the pathway preceding full oxidation of glucose remains unclear. The importance of glucose transport in neurons has been demonstrated in a number of recent studies (54), that challenge the well-established astrocyte neuron lactate shuttle (ANSL) hypothesis (55), to suggest that glucose is the major substrate for the normal, activated brain. Our data suggest that glucose uptake is increased in LPL depleted neurons. Whether this altered substrate utilization is a compensatory response to reduced lipid uptake following LPL loss is likely but remains to be determined.

FLIM analysis of endogenous neuronal metabolism in PVN neurons also revealed a marked increase in free FAD (Fig. 4E). This suggests an increased flux through pathways in which free FAD would be produced (e.g. complex II activity in the TCA (28)), and reduced flux through pathways in which FAD would be enzyme-bound (e.g. FA oxidation). This suggested partitioning, is consistent with increased glucose uptake and utilization, driving the oxidative metabolism of glucose and/or its intermediary metabolites (i.e. lactate) during reduced FA uptake and oxidation following LPL loss.

Hypothalamic neurons, in specific sub-nuclei sense the abundance of leptin, insulin, neuropeptides and FAs (36, 56–58), which may result in ATP-dependent potassium channel activation. Although neurons are thought to rely primarily on the oxidative metabolism of glucose/lactate to fulfill bioenergetics needs, fatty acid oxidation may also be important for the metabolism and function of hypothalamic neurons.

For example, the inhibition CPT-1 activity in the hypothalamus results in a reduced neuronal FA oxidation and increased accumulation of long chain fatty acids (LC-FAs) (59). This shift in metabolism may signal a “fed state” resulting in marked inhibition in food intake and reduced nutrient mobilization, i.e. EGP (59). It is thought that the accumulation of malonyl-CoA may play a key role in neuronal FA sensing, since inhibition of fatty acid synthase can suppress food intake in a malonyl-CoA dependent manner (60). In addition, malonyl-CoA is potent inhibitor of CPT-1 and thus LC-FA oxidation. Here, we show that LPL-depleted neurons in the PVN show increased free NADH and FAD which is consistent with a metabolic shift away from mitochondrial FA oxidation of LC-FAs (Fig. 4D-E). In addition, we clearly demonstrate that neuronal cell lines lacking LPL have diminished accumulation of the LC-PUFAs, whereas neuronal cell lines that over express LPL have increased accumulation of LC-PUFAs, such as ETA, EPA and DHA (Fig. 5C). Importantly, these data recapitulate our findings in vivo, showing reduced LC-PUFA abundance in the brains of NEXLPL-/-, and NEXLPL-/+ mice (11, 13), and highlight the utility of this cell line for investigating underlying metabolic changes following LPL modulation. Moreover, these data suggest that LPL is involved in neuronal uptake of LC-PUFAs, which may be an important signal in the regulation of hepatic metabolism and nutrient mobilization. Findings from existing literature would suggest that neuronal LC-PUFAs depletion may signal poor nutrient availability to stimulate increased food intake and increased EGP (59). While our data are in part consistent with this notion, these studies have all been acute responses to modulated FA sensing, and do not take into the account the potential for compensatory mechanisms that occur with aging. For example, it is plausible that long-term changes in essential FA uptake have a larger impact over time that the response to acute changes in nutrient availability. It is well established LC-PUFAs are found in either the C1 or C2 position of major phospholipid species that play critical roles in neuronal functions such as growth, signaling, and excitatory and inhibitory synaptic transmission (61). Therefore, long-term reductions in LPL-mediated LC-PUFA uptake may have profound effects on synaptic transmission and neuronal maintenance over time. Whether these translate to downstream changes in systemic metabolism will be an important focus of future work.

7. Conclusion

The path to T2DM involves increased hepatic lipid accumulation, hepatic insulin resistance and increased EGP. Since the ANS can regulate hepatic metabolism, it offers a novel therapeutic target for NAFLD and T2DM. However, mechanisms related to neuronal inputs to the ANS control of hepatic metabolism remain unclear. Here, we have shown surprisingly that mice with neuronal LPL deficiency and obesity show improvements in glucose tolerance with aging. Moreover, these changes are associated with reduced hepatic lipid content and altered synaptic activity of liver-related neurons in the PVN of the hypothalamus. Loss of LPL has a marked effect on neuronal metabolism and can shift substrate utilization towards glucose oxidation in the absence of LC-PUFA transport. Our findings suggest that neuronal LPL is a key component of liver-related preautonomic neurons and highlight the modulation of neuronal lipid metabolism as an intervention strategy to preserve insulin sensitivity in the aged and obese.

8. List Of Abbrevaitions

Lon-alcoholic fatty liver disease (NAFLD)

Lipoprotein lipase (LPL)

Paraventricular nucleus (PVN)

Fluorescence Lifetime Imaging Microscopy (FLIM)

Stearoyl-CoA desaturase-1 (SCD1)

Acyl-CoA 6-desaturase (FADS2)

Nicotinamide Adenine Dinucleotide (NADH)

Flavin Adenine Dinucleotide (FAD)

Tricarboxylic acid cycle (TCA)

Type 2 diabetes mellitus (T2DM)

Autonomic nervous system (ANS)

Very low density Lipoprotein TG (VLDL-TG)

Triglycerides (TG)

Fatty acids (FA)

Polyunsaturated fatty acids (PUFA)

Fatty acid methyl ester (FAME)

Polymerase Chain reaction (PCR)

Glyceraldehyde 3-phosphate dehydrogenase (GAPDH)

Beta-actin (ACTB)

Enhanced green fluorescent protein (EGFP)

Artificial cerebrospinal fluid (aCSF)

Calmodulin-dependent protein kinase II (CaMKIIa)

Adeno-Associated virus Serotype 8 (AAV8)

Murine Stem cell virus (MSCV)

Small hairpin RNA (shRNA)

Ultra high performance liquid chromatography (UHPLC)

Analysis of Variance (ANOVA)

Intraperitoneal (IP)

Glucose tolerance tests (GTT)

Endogenous glucose production (EGP)

Monounsaturated Fatty acid (MUFA)

Low density lipoprotein (LDL)

Pentose phosphate pathway (PPP)

Insulin-sensitive obese (ISO)

Sympathetic nervous system [SNS]

Parasympathetic nervous system [PNS]

Astrocyte neuron lactate shuttle (ANSL)

Declarations

Acknowledgements. The authors would like to thank Rachel Janssen and the molecular and cellular analytical core at University of Colorado Anschutz medical campus for technical assistance during gene expression studies. The authors would also like to thank the metabolomics core at University of Colorado Anschutz medical campus for technical assistance during global metabolomics analysis. Imaging experiments were performed in the University of Colorado Anschutz Medical Campus Advanced Light Microscopy Core supported in part by NIH/NCATS Colorado CTSI Grant Number UL1 TR001082.

Funding. This work was supported with funds from the NIH awarded to K.D.B (5KL2TR002534-02) R.H.E (R01 DK089309-01A1) and A.Z (R01 DK099598-01A1).

Duality of Interest. There are no conflicts of interest relevant to this article.

Author Contributions. K.D.B designed experiments, performed experiments, analyzed data, and wrote the paper. E. D., T.Y., S.G., A.E.L., H.G., performed experiments, analyzed data and edited the paper. H.W., designed experiments, performed experiments and analyzed data. A.Z., designed experiments, analyzed data and wrote the paper. R.H.E designed experiments and edited the paper.

References

1. Bril, F., and Cusi, K. (2017) Management of Nonalcoholic Fatty Liver Disease in Patients With Type 2 Diabetes: A Call to Action. *Diabetes Care* **40**, 419-430
2. Fabbrini, E., Sullivan, S., and Klein, S. (2010) Obesity and nonalcoholic fatty liver disease: biochemical, metabolic, and clinical implications. *Hepatology* **51**, 679-689
3. Perry, R. J., Samuel, V. T., Petersen, K. F., and Shulman, G. I. (2014) The role of hepatic lipids in hepatic insulin resistance and type 2 diabetes. *Nature* **510**, 84-91
4. Yki-Jarvinen, H. (2014) Non-alcoholic fatty liver disease as a cause and a consequence of metabolic syndrome. *Lancet Diabetes Endocrinol* **2**, 901-910
5. Ribeiro, I. M. R., and Antunes, V. R. (2018) The role of insulin at brain-liver axis in the control of glucose production. *Am J Physiol Gastrointest Liver Physiol* **315**, G538-G543
6. Lam, T. K., Gutierrez-Juarez, R., Pocai, A., Bhanot, S., Tso, P., Schwartz, G. J., and Rossetti, L. (2007) Brain glucose metabolism controls the hepatic secretion of triglyceride-rich lipoproteins. *Nat Med* **13**, 171-180
7. Yue, J. T., Abraham, M. A., LaPierre, M. P., Mighiu, P. I., Light, P. E., Filippi, B. M., and Lam, T. K. (2015) A fatty acid-dependent hypothalamic-DVC neurocircuitry that regulates hepatic secretion of triglyceride-rich lipoproteins. *Nat Commun* **6**, 5970
8. Song, B. J., Elbert, A., Rahman, T., Orr, S. K., Chen, C. T., Febbraio, M., and Bazinet, R. P. (2010) Genetic ablation of CD36 does not alter mouse brain polyunsaturated fatty acid concentrations. *Lipids* **45**, 291-299
9. Laperrousaz, E., Moulle, V. S., Denis, R. G., Kassis, N., Berland, C., Colsch, B., Fioramonti, X., Philippe, E., Lacombe, A., Vanacker, C., Butin, N., Bruce, K. D., Wang, H., Wang, Y., Gao, Y., Garcia-Caceres, C., Prevot, V., Tschop, M. H., Eckel, R. H., Le Stunff, H., Luquet, S., Magnan, C., and Cruciani-Guglielmacci, C. (2017) Lipoprotein lipase in hypothalamus is a key regulator of body weight gain and glucose homeostasis in mice. *Diabetologia* **60**, 1314-1324
10. Libby, A. E., Wang, H., Mittal, R., Sungelo, M., Potma, E., and Eckel, R. H. (2015) Lipoprotein lipase is an important modulator of lipid uptake and storage in hypothalamic neurons. *Biochem Biophys Res Commun* **465**, 287-292
11. Wang, H., Astarita, G., Taussig, M. D., Bharadwaj, K. G., DiPatrizio, N. V., Nave, K. A., Piomelli, D., Goldberg, I. J., and Eckel, R. H. (2011) Deficiency of lipoprotein lipase in neurons modifies the regulation of energy balance and leads to obesity. *Cell Metab* **13**, 105-113
12. Wang, H., Taussig, M. D., DiPatrizio, N. V., Bruce, K., Piomelli, D., and Eckel, R. H. (2016) Obesity development in neuron-specific lipoprotein lipase deficient mice is not responsive to increased dietary fat content or change in fat composition. *Metabolism* **65**, 987-997
13. Yu, T., Taussig, M. D., DiPatrizio, N. V., Astarita, G., Piomelli, D., Bergman, B. C., Dell'Acqua, M. L., Eckel, R. H., and Wang, H. (2015) Deficiency of Lipoprotein Lipase in Neurons Decreases AMPA Receptor Phosphorylation and Leads to Neurobehavioral Abnormalities in Mice. *PLoS One* **10**, e0135113

14. Kim, H. J., Higashimori, T., Park, S. Y., Choi, H., Dong, J., Kim, Y. J., Noh, H. L., Cho, Y. R., Cline, G., Kim, Y. B., and Kim, J. K. (2004) Differential effects of interleukin-6 and -10 on skeletal muscle and liver insulin action in vivo. *Diabetes* **53**, 1060-1067
15. Libby, A. E., Bales, E., Orlicky, D. J., and McManaman, J. L. (2016) Perilipin-2 Deletion Impairs Hepatic Lipid Accumulation by Interfering with Sterol Regulatory Element-binding Protein (SREBP) Activation and Altering the Hepatic Lipidome. *J Biol Chem* **291**, 24231-24246
16. Orlicky, D. J., Libby, A. E., Bales, E. S., McMahan, R. H., Monks, J., La Rosa, F. G., and McManaman, J. L. (2019) Perilipin-2 promotes obesity and progressive fatty liver disease in mice through mechanistically distinct hepatocyte and extra-hepatocyte actions. *J Physiol* **597**, 1565-1584
17. Libby, A. E., Bales, E. S., Monks, J., Orlicky, D. J., and McManaman, J. L. (2018) Perilipin-2 deletion promotes carbohydrate-mediated browning of white adipose tissue at ambient temperature. *J Lipid Res* **59**, 1482-1500
18. Bruce, K. D., Cagampang, F. R., Argenton, M., Zhang, J., Ethirajan, P. L., Burdge, G. C., Bateman, A. C., Clough, G. F., Poston, L., Hanson, M. A., McConnell, J. M., and Byrne, C. D. (2009) Maternal high-fat feeding primes steatohepatitis in adult mice offspring, involving mitochondrial dysfunction and altered lipogenesis gene expression. *Hepatology* **50**, 1796-1808
19. Jenkins, A. J., Lyons, T. J., Zheng, D., Otvos, J. D., Lackland, D. T., McGee, D., Garvey, W. T., Klein, R. L., and Group, D. E. R. (2003) Serum lipoproteins in the diabetes control and complications trial/epidemiology of diabetes intervention and complications cohort: associations with gender and glycemia. *Diabetes Care* **26**, 810-818
20. Gao, H., Miyata, K., Bhaskaran, M. D., Derbenev, A. V., and Zsombok, A. (2012) Transient receptor potential vanilloid type 1-dependent regulation of liver-related neurons in the paraventricular nucleus of the hypothalamus diminished in the type 1 diabetic mouse. *Diabetes* **61**, 1381-1390
21. Gao, H., Molinas, A. J. R., Miyata, K., Qiao, X., and Zsombok, A. (2017) Overactivity of Liver-Related Neurons in the Paraventricular Nucleus of the Hypothalamus: Electrophysiological Findings in db/db Mice. *J Neurosci* **37**, 11140-11150
22. Zsombok, A., Gao, H., Miyata, K., Issa, A., and Derbenev, A. V. (2011) Immunohistochemical localization of transient receptor potential vanilloid type 1 and insulin receptor substrate 2 and their co-localization with liver-related neurons in the hypothalamus and brainstem. *Brain Res* **1398**, 30-39
23. Krashes, M. J., Shah, B. P., Madara, J. C., Olson, D. P., Strochlic, D. E., Garfield, A. S., Vong, L., Pei, H., Watabe-Uchida, M., Uchida, N., Liberles, S. D., and Lowell, B. B. (2014) An excitatory paraventricular nucleus to AgRP neuron circuit that drives hunger. *Nature* **507**, 238-242
24. Berezin, M. Y., and Achilefu, S. (2010) Fluorescence lifetime measurements and biological imaging. *Chem Rev* **110**, 2641-2684
25. Digman, M. A., Caiolfa, V. R., Zamai, M., and Gratton, E. (2008) The phasor approach to fluorescence lifetime imaging analysis. *Biophys J* **94**, L14-16
26. Marwan, A. I., Shabeka, U., Reisz, J. A., Zheng, C., Serkova, N. J., and Dobrinskikh, E. (2018) Unique Heterogeneous Topological Pattern of the Metabolic Landscape in Rabbit Fetal Lungs following

Tracheal Occlusion. *Fetal Diagn Ther*

27. Dobrinskikh, E., Al-Juboori, S. I., Shabeka, U., Reisz, J. A., Zheng, C., and Marwan, A. I. (2019) Heterogeneous Pulmonary Response After Tracheal Occlusion: Clues to Fetal Lung Growth. *J Surg Res* **239**, 242-252
28. Wallrabe, H., Svindrych, Z., Alam, S. R., Siller, K. H., Wang, T., Kashatus, D., Hu, S., and Periasamy, A. (2018) Segmented cell analyses to measure redox states of autofluorescent NAD(P)H, FAD & Trp in cancer cells by FLIM. *Sci Rep* **8**, 79
29. McCurdy, C. E., Schenk, S., Hetrick, B., Houck, J., Drew, B. G., Kaye, S., Lashbrook, M., Bergman, B. C., Takahashi, D. L., Dean, T. A., Nemkov, T., Gertsman, I., Hansen, K. C., Philp, A., Hevener, A. L., Chicco, A. J., Aagaard, K. M., Grove, K. L., and Friedman, J. E. (2016) Maternal obesity reduces oxidative capacity in fetal skeletal muscle of Japanese macaques. *JCI Insight* **1**, e86612
30. Nemkov, T., Hansen, K. C., and D'Alessandro, A. (2017) A three-minute method for high-throughput quantitative metabolomics and quantitative tracing experiments of central carbon and nitrogen pathways. *Rapid Commun Mass Spectrom* **31**, 663-673
31. Nemkov, T., D'Alessandro, A., and Hansen, K. C. (2015) Three-minute method for amino acid analysis by UHPLC and high-resolution quadrupole orbitrap mass spectrometry. *Amino Acids* **47**, 2345-2357
32. Gunion, M. W., Tache, Y., Rosenthal, M. J., Miller, S., Butler, B., and Zib, B. (1989) Bombesin microinfusion into the rat hypothalamic paraventricular nucleus increases blood glucose, free fatty acids and corticosterone. *Brain Res* **478**, 47-58
33. Ionescu, E., Coimbra, C. C., Walker, C. D., and Jeanrenaud, B. (1989) Paraventricular nucleus modulation of glycemia and insulinemia in freely moving lean rats. *Am J Physiol* **257**, R1370-1376
34. Kalsbeek, A., La Fleur, S., Van Heijningen, C., and Buijs, R. M. (2004) Suprachiasmatic GABAergic inputs to the paraventricular nucleus control plasma glucose concentrations in the rat via sympathetic innervation of the liver. *J Neurosci* **24**, 7604-7613
35. Magistretti, P. J., and Allaman, I. (2015) A cellular perspective on brain energy metabolism and functional imaging. *Neuron* **86**, 883-901
36. Bruinstroop, E., Pei, L., Ackermans, M. T., Foppen, E., Borgers, A. J., Kwakkel, J., Alkemade, A., Fliers, E., and Kalsbeek, A. (2012) Hypothalamic neuropeptide Y (NPY) controls hepatic VLDL-triglyceride secretion in rats via the sympathetic nervous system. *Diabetes* **61**, 1043-1050
37. Cheng, L., Yu, Y., Szabo, A., Wu, Y., Wang, H., Camer, D., and Huang, X. F. (2015) Palmitic acid induces central leptin resistance and impairs hepatic glucose and lipid metabolism in male mice. *J Nutr Biochem* **26**, 541-548
38. Obici, S., Feng, Z., Karkanias, G., Baskin, D. G., and Rossetti, L. (2002) Decreasing hypothalamic insulin receptors causes hyperphagia and insulin resistance in rats. *Nat Neurosci* **5**, 566-572
39. Denis, G. V., and Hamilton, J. A. (2013) Healthy obese persons: how can they be identified and do metabolic profiles stratify risk? *Curr Opin Endocrinol Diabetes Obes* **20**, 369-376
40. Bluher, M. (2010) The distinction of metabolically 'healthy' from 'unhealthy' obese individuals. *Curr Opin Lipidol* **21**, 38-43

41. Samocha-Bonet, D., Chisholm, D. J., Tonks, K., Campbell, L. V., and Greenfield, J. R. (2012) Insulin-sensitive obesity in humans - a 'favorable fat' phenotype? *Trends Endocrinol Metab* **23**, 116-124
42. Shimazu, T. (1967) Glycogen synthetase activity in liver: regulation by the autonomic nerves. *Science* **156**, 1256-1257
43. Shimazu, T. (1971) Regulation of glycogen metabolism in liver by the autonomic nervous system. V. Activation of glycogen synthetase by vagal stimulation. *Biochim Biophys Acta* **252**, 28-38
44. Sigala, B., McKee, C., Soeda, J., Pazienza, V., Morgan, M., Lin, C. I., Selden, C., Vander Borght, S., Mazzoccoli, G., Roskams, T., Vinciguerra, M., and Oben, J. A. (2013) Sympathetic nervous system catecholamines and neuropeptide Y neurotransmitters are upregulated in human NAFLD and modulate the fibrogenic function of hepatic stellate cells. *PLoS One* **8**, e72928
45. Hurr, C., Simonyan, H., Morgan, D. A., Rahmouni, K., and Young, C. N. (2019) Liver sympathetic denervation reverses obesity-induced hepatic steatosis. *J Physiol*
46. O'Hare, J. D., and Zsombok, A. (2016) Brain-liver connections: role of the preautonomic PVN neurons. *Am J Physiol Endocrinol Metab* **310**, E183-189
47. Friedman, J. E., Dobrinskikh, E., Alfonso-Garcia, A., Fast, A., Janssen, R. C., Soderborg, T. K., Anderson, A. L., Reisz, J. A., D'Alessandro, A., Frank, D. N., Robertson, C. E., de la Houssaye, B. A., Johnson, L. K., Orlicky, D. J., Wang, X. X., Levi, M., Potma, E. O., El Kasmi, K. C., and Jonscher, K. R. (2018) Pyrroloquinoline quinone prevents developmental programming of microbial dysbiosis and macrophage polarization to attenuate liver fibrosis in offspring of obese mice. *Hepatol Commun* **2**, 313-328
48. Ranjit, S., Dvornikov, A., Dobrinskikh, E., Wang, X., Luo, Y., Levi, M., and Gratton, E. (2017) Measuring the effect of a Western diet on liver tissue architecture by FLIM autofluorescence and harmonic generation microscopy. *Biomed Opt Express* **8**, 3143-3154
49. Stringari, C., Nourse, J. L., Flanagan, L. A., and Gratton, E. (2012) Phasor fluorescence lifetime microscopy of free and protein-bound NADH reveals neural stem cell differentiation potential. *PLoS One* **7**, e48014
50. Drozdowicz-Tomsia, K., Anwer, A. G., Cahill, M. A., Madlum, K. N., Maki, A. M., Baker, M. S., and Goldys, E. M. (2014) Multiphoton fluorescence lifetime imaging microscopy reveals free-to-bound NADH ratio changes associated with metabolic inhibition. *J Biomed Opt* **19**, 086016
51. Ranjit, S., Malacrida, L., Stakic, M., and Gratton, E. (2019) Determination of the metabolic index using the fluorescence lifetime of free and bound NADH in the phasor approach. *J Biophotonics*, e201900156
52. Bolanos, J. P., Almeida, A., and Moncada, S. (2010) Glycolysis: a bioenergetic or a survival pathway? *Trends Biochem Sci* **35**, 145-149
53. Herrero-Mendez, A., Almeida, A., Fernandez, E., Maestre, C., Moncada, S., and Bolanos, J. P. (2009) The bioenergetic and antioxidant status of neurons is controlled by continuous degradation of a key glycolytic enzyme by APC/C-Cdh1. *Nat Cell Biol* **11**, 747-752

54. Dienel, G. A. (2012) Brain lactate metabolism: the discoveries and the controversies. *J Cereb Blood Flow Metab* **32**, 1107-1138
55. Pellerin, L., and Magistretti, P. J. (1994) Glutamate uptake into astrocytes stimulates aerobic glycolysis: a mechanism coupling neuronal activity to glucose utilization. *Proc Natl Acad Sci U S A* **91**, 10625-10629
56. Broberger, C., Visser, T. J., Kuhar, M. J., and Hokfelt, T. (1999) Neuropeptide Y innervation and neuropeptide-Y-Y1-receptor-expressing neurons in the paraventricular hypothalamic nucleus of the mouse. *Neuroendocrinology* **70**, 295-305
57. Pocai, A., Lam, T. K., Gutierrez-Juarez, R., Obici, S., Schwartz, G. J., Bryan, J., Aguilar-Bryan, L., and Rossetti, L. (2005) Hypothalamic K(ATP) channels control hepatic glucose production. *Nature* **434**, 1026-1031
58. van den Hoek, A. M., van Heijningen, C., Schroder-van der Elst, J. P., Ouwens, D. M., Havekes, L. M., Romijn, J. A., Kalsbeek, A., and Pijl, H. (2008) Intracerebroventricular administration of neuropeptide Y induces hepatic insulin resistance via sympathetic innervation. *Diabetes* **57**, 2304-2310
59. Obici, S., Feng, Z., Arduini, A., Conti, R., and Rossetti, L. (2003) Inhibition of hypothalamic carnitine palmitoyltransferase-1 decreases food intake and glucose production. *Nat Med* **9**, 756-761
60. Loftus, T. M., Jaworsky, D. E., Frehywot, G. L., Townsend, C. A., Ronnett, G. V., Lane, M. D., and Kuhajda, F. P. (2000) Reduced food intake and body weight in mice treated with fatty acid synthase inhibitors. *Science* **288**, 2379-2381
61. Bazan, N. G. (2003) Synaptic lipid signaling: significance of polyunsaturated fatty acids and platelet-activating factor. *J Lipid Res* **44**, 2221-2233

Supplemental Figures

Supplemental Figure 1: https://figshare.com/s/d125253ec0dfc4eafc81

Supplemental Figure 2: https://figshare.com/s/a17b4d86cb6dafe10949

Supplemental Figure 3: https://figshare.com/s/cc5b4597659171c99eda

Figures

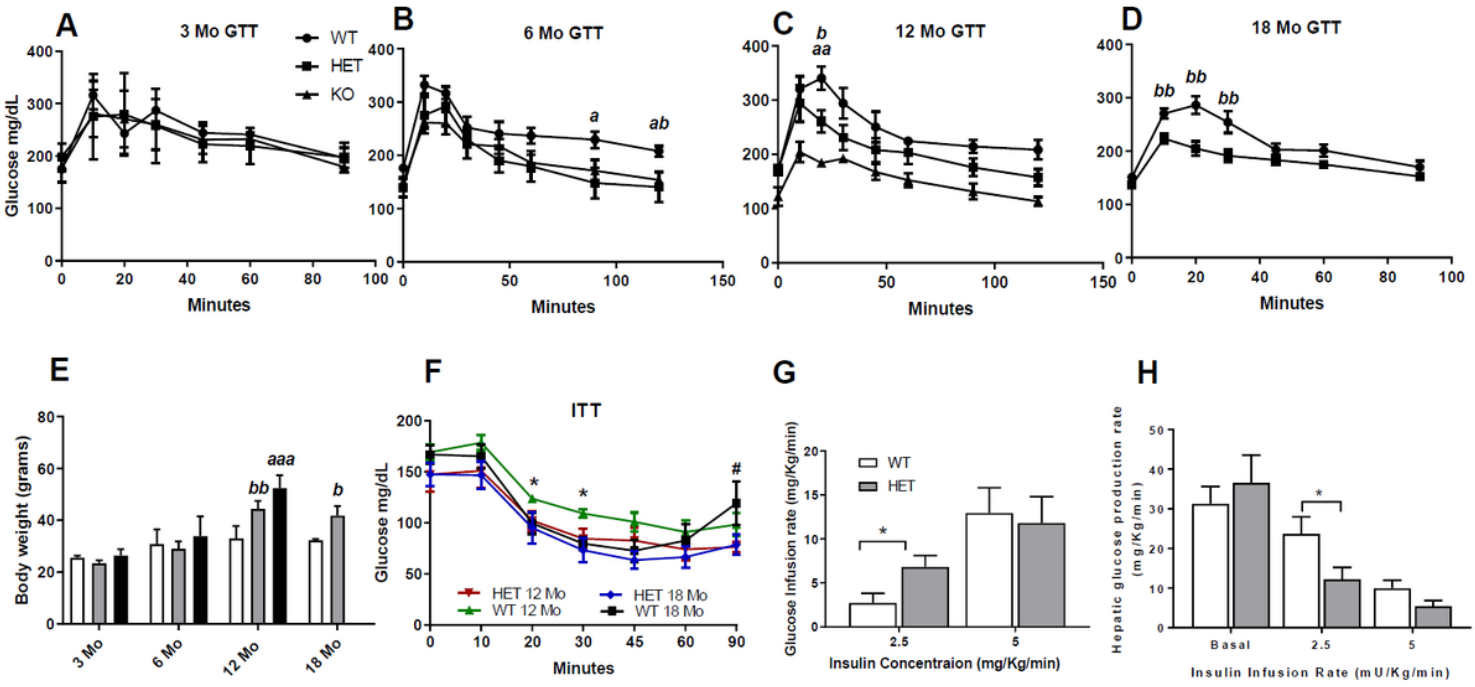

Figure 1

Neuronal Lipoprotein deficiency improves Glucose tolerance. A-D. Measurements of glucose tolerance in NEXLPL+/-, NEXLPL-/- and WT mice at 3 (A), 6 (B), 12 (C) and 18 (D) mo. E. The body weights of NEXLPL+/- (Grey), NEXLPL-/- (black) and WT (white) mice before terminal experiments at each age point. a = P<0.05 vs WT and NEXLPL-/-, aa = P<0.01 vs WT and NEXLPL-/-, b = P<0.05 versus WT and NEXLPL+/-, bb = P<0.01 vs WT and NEXLPL+/-. F. IP insulin tolerance tests in 12 and 18 mo. NEXLPL+/- and WT mice. G. Steady state whole body glucose infusion rate in NEXLPL+/- (grey) mice compared to WT (white). H. Endogenous glucose production (EGP) rate in the NEXLPL+/- mice compared to WT controls. (Where # = P<0.1 vs WT and * = P<0.05 vs WT of aged-matched animals)

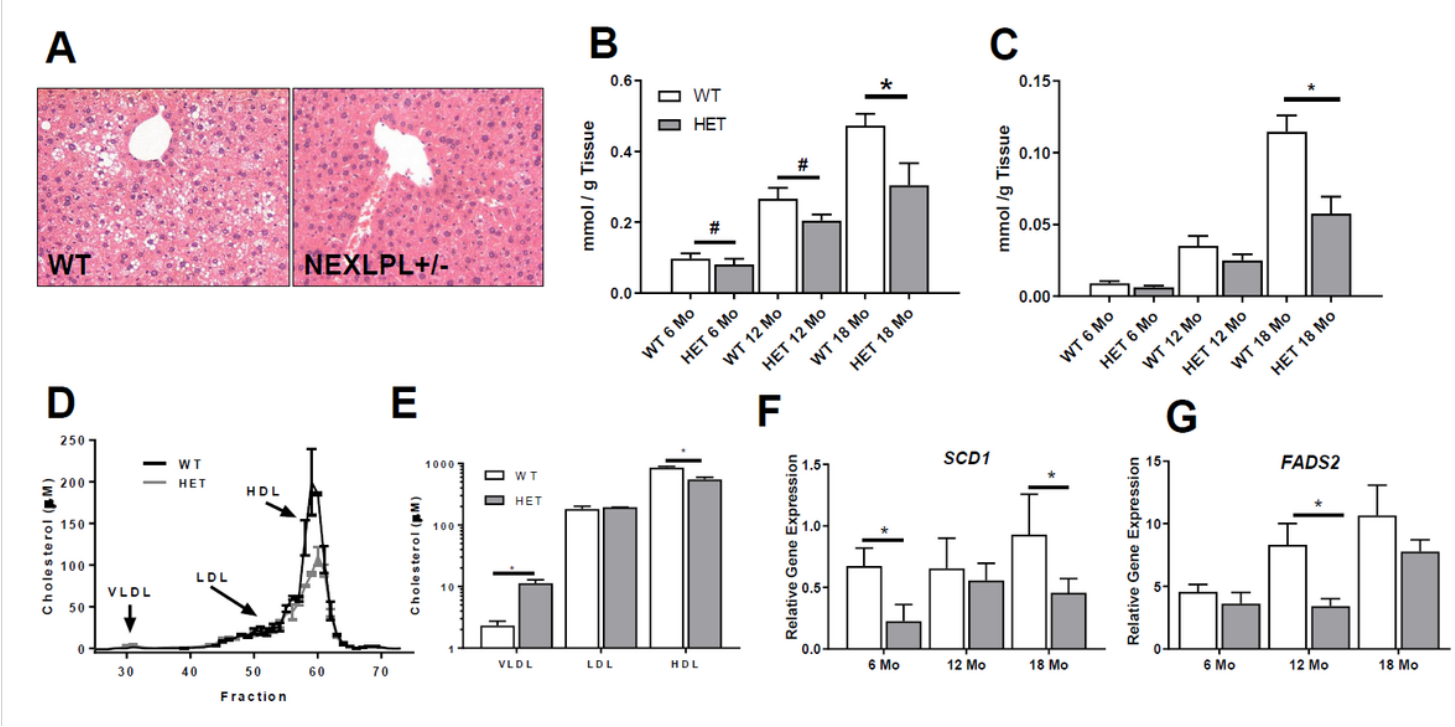

Figure 2

Hepatic lipid accumulation is reduced in mice heterozygous for LPL deficiency. A. H and E stained liver of 6 mo. WT and NEXLPL+/- mice. B. Hepatic triglyceride (TG) concentration is reduced in NEXLPL+/- (grey bars) compared to WT mice (white bars). C. Hepatic mono-unsaturated fatty acid (MUFA) concentration is reduced in NEXLPL+/- mice. D. FPLC fractionation of lipoproteins from plasma of NEXLPL+/- and WT mice. E. Cholesterol content of lipoprotein fractions from 6 mo mice. F. Relative gene expression of SCD1. G. Relative gene expression of FADS2. (* = P<0.05 vs WT, of corresponding age).

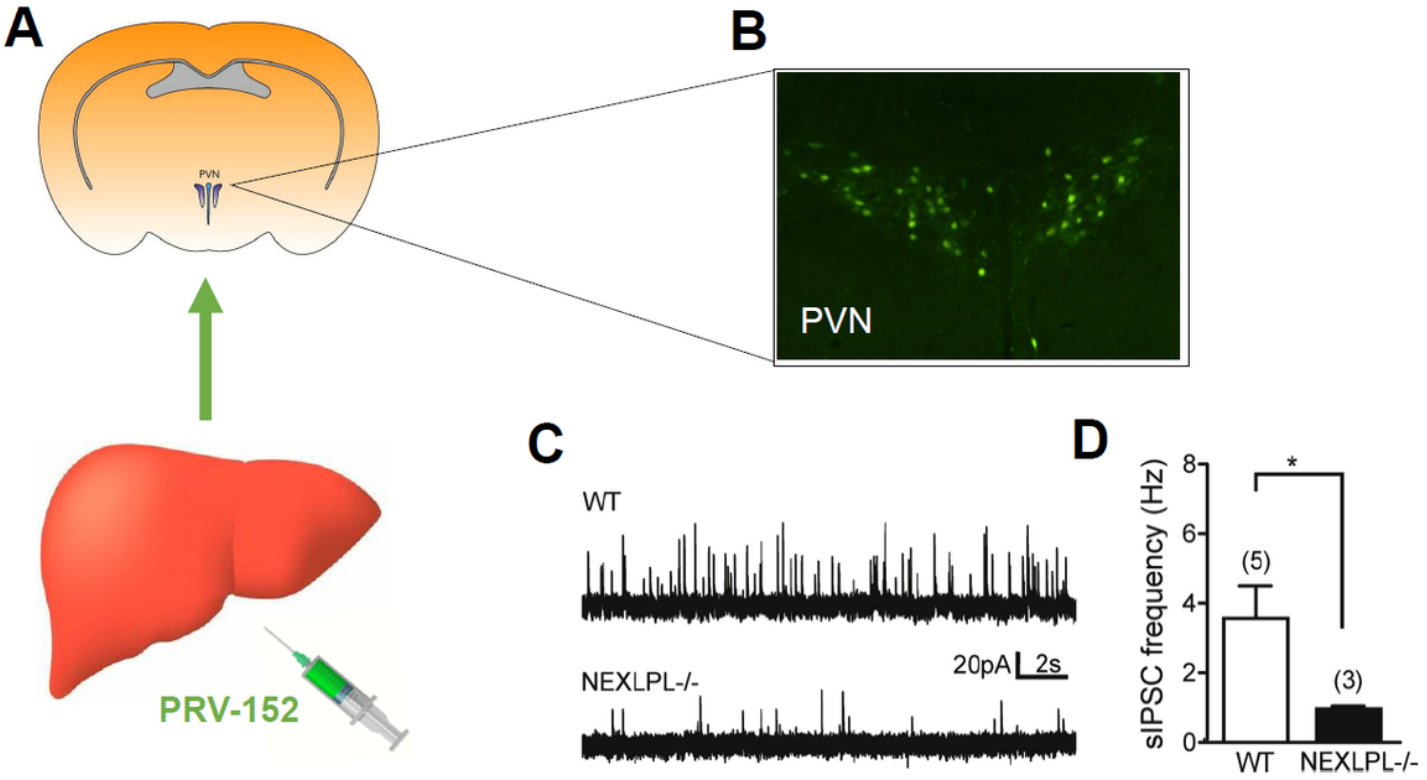

Figure 3

Decreased inhibitory synaptic regulation of liver-related PVN neurons in NEXLPL-/- mice. A-B. Liver-related neurons in the PVN were identified with a retrograde transsynaptic viral tracer (PRV-152), and used for patch-clamp recordings. C. Recordings of sIPSCs in WT and NEXLPL-/- mice. D. The frequency of sIPSCs was reduced in NEXLPL-/- mice compared to WT mice. (* = P<0.05 vs WT)

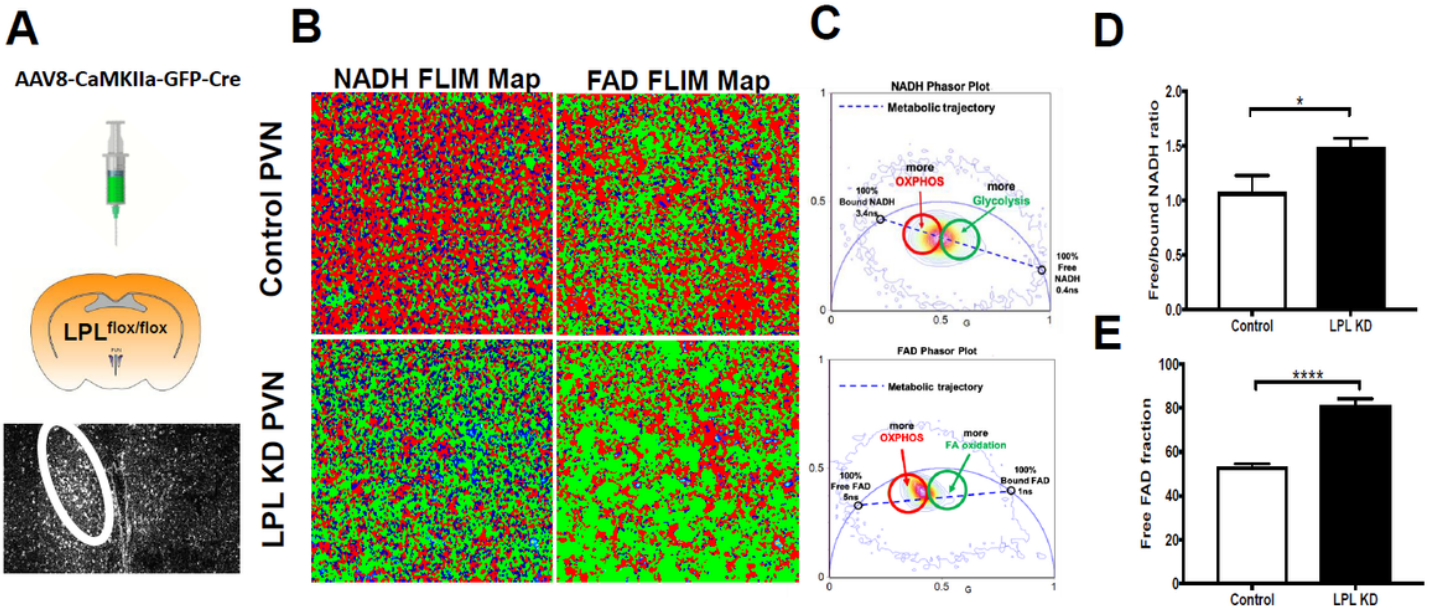

Figure 4

Depletion of LPL in PVN neurons results in altered metabolic flux. A. LPL was depleted in the PVN of LPLflox/flox by the delivery of AAV8-CaMKIIa-GFP-Cre, whereas AAV8-CaMKIIa-GFP was administered to control mice. B. Representative images of NADH and FAD FLIM Maps from images of the PVN in Control versus LPL KD Mice. C. Phasor plots, showing the shift in metabolic trajectory with changing lifetime for NADH and FAD. D. Increased ratio of free/bound NADH in LPL KD PVN neurons. E. Increased free FAD fraction in LPL KD PVN neurons. (* = P<0.05 vs WT, ****= P<0.0001 vs WT)

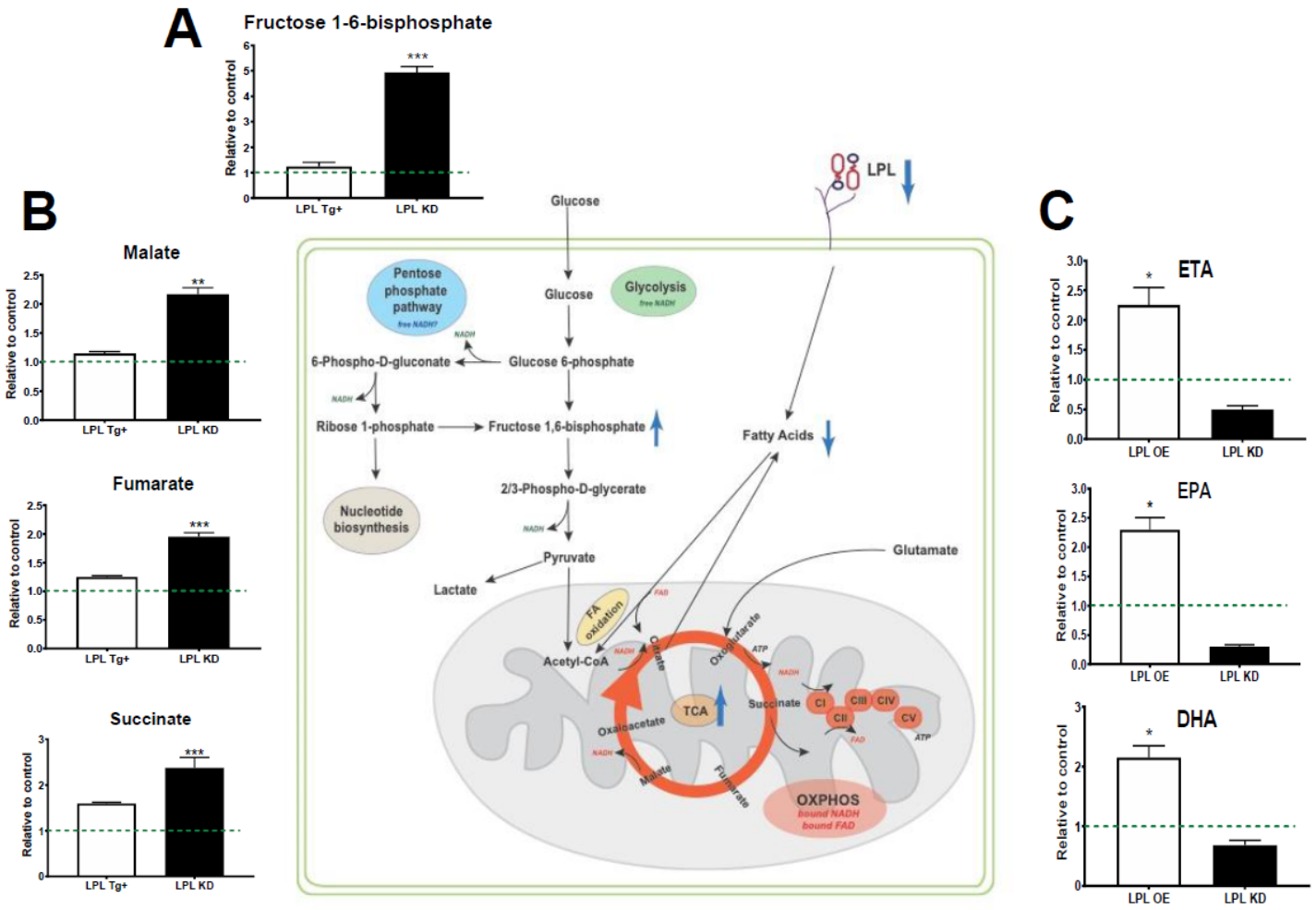

Figure 5

Altered substrate utilization in hypothalamic neurons deficient in or over –expressing LPL. A. LPL KD N41 neurons show increased abundance of Fructose 1-6 bisphosphate. B. LPL KD N41 neurons show increased TCA intermediates. C. LPL OE N41 neurons have increased abundance of LC-PUFAs. * = P<0.05 vs WT, ** = P<0.01 vs WT, *** = P<0.001 vs WT.